NUKLEONIKA 2015;60(1):15–18
doi: 10.1515/nuka-2015-0005

ORIGINAL PAPER

DE GRUYTER
OPEN

The microstructure and magnetic properties of $Nd_{8.5}Tb_{1.5}Fe_{83}Zr_1B_6$ ribbons obtained at various cooling rates

Marcin Dośpiał, Jacek Olszewski, Marcin Nabiałek, Paweł Pietrusiewicz, Tomasz Kaczmarzyk

Abstract. The paper presents results of microstructure and magnetic properties studies of $Nd_{8.5}Tb_{1.5}Fe_{83}Zr_1B_6$ ribbons obtained by melt-spinning technique. The samples were produced using the rapid cooling of liquid alloy on the copper wheel, by applying three different linear velocities 20, 30, and 35 m/s. The microstructure of obtained ribbons was examined using X-ray diffractometry and Mössbauer spectroscopy. Magnetic measurements were performed using LakeShore vibrating sample magnetometer. The microstructure measurements were used for quantitative and qualitative analysis of phase composition. Basing on results of structure studies combined with magnetic measurements, the influence of phase composition on hysteresis loop behavior was described.

Key words: microstructure analysis • Mössbauer spectroscopy • permanent magnets • reversal magnetization

M. Dośpiał✉, J. Olszewski, M. Nabiałek,
P. Pietrusiewicz, T. Kaczmarzyk
Institute of Physics,
Czestochowa University of Technology,
19 Armii Krajowej Ave., 42-200 Czestochowa, Poland,
Tel.: +48 34 325 0610, Fax: +48 34 325 0795,
E-mail: mdospial@wp.pl

Received: 18 June 2014
Accepted: 28 July 2014

Introduction

Modern Re-Fe-B hard magnetic materials, produced using rapid quenching technique, taking into account variations in chemical composition, can be divided into three groups i.e. of stoichiometric, $Re_2Fe_{14}B$ composition, and with excess of rare earth or iron [1–3].

Materials, composed of Re-Fe-B compound with overstoichiometric rare earths, typically are characterized by worse glass transition ability, smallest M_r/M_s ratio and large coercivity. Their properties are shaped by exchange interactions between $Re_2Fe_{14}B$, which are weakened by an increased distance between the grains. Enlarged distance between grains is resulting from the presence of a thin boundary formed from an amorphous matrix of redundant rare earths. Additionally, the presence of such a boundary causes an increase in coercivity due to the strong bonding of domain walls at the grain boundaries [4]. The stoichiometric composition causes increase in glass transition ability, M_r/M_s ratio but also causes deterioration of coercivity. These changes are a result of a reduction in the distance between grains, by removing the paramagnetic amorphous matrix, and finer structure as a result of increase in glass transition ability [5]. The highest glass transition ability, finer structure and highest M_r/M_s ratio is met in Re-Fe-B compound with overstoichiometric iron. The significantly higher value of the M_r/M_s ratio results from the presence of the strong exchange interactions, between particles that differ in magnetic hardness. The grains, of soft magnetic phase, have

a much smaller size and are completely covered by the exchange interactions. Unfortunately, these materials have the lowest coercivity [6]. In order to compensate the decreasing in coercivity caused by the exchange interaction, the typically used rare earths atoms (Nd, Pr) are replaced by a small amount of terbium (Tb = 0.5–2 at.%), since the anisotropy field of $Tb_2Fe_{14}B$ phase is higher than the anisotropy field of $Nd_2Fe_{14}B$ phase [7, 8].

A slightly stronger exchange coupling as for group of crystalline materials based on a Re-Fe-B compound with an excessive amount of iron is observed for partly crystallized materials with the same composition.

This work is focused on the study of effect of the copper drum linear speed on the phase composition of the alloy with an excess amount of iron. Proper selection of the linear velocity allows obtaining content ratio of the $Nd_2Fe_{14}B$ crystalline phase to the amorphous matrix, which enables coupling of the magnetic moments of amorphous matrix and of $Nd_2Fe_{14}B$ grains by strong exchange interactions. Through an existence of such coupling it is possible to obtain a material with extremely good and hard magnetic properties.

Experimental procedure

The samples of $Nd_{8.5}Tb_{1.5}Fe_{83}Zr_1B_6$ were obtained from high purity elements using the arc melting in the protective argon atmosphere. A small amount of Zr (1 at.%) was added in order to hinder the grain growth. The nanocomposite ribbons were prepared by rapid quenching of the liquid alloy on a rotating cooper wheel for three different linear velocities 20, 30, and 35 m/s. Both ingots and the samples were prepared in protective gas atmosphere under the pressure inside the chamber of 0.4×10^5 Pa.

The XRD patterns were carried out using a 'Bruker' X-ray diffractometer equipped with a Lynx Eye semiconductor counter. Diffraction patterns were made using CuK_α radiation source of characteristic wave length 1.541 Å in Bragg–Brentano geometry. Samples for X-ray measurements were scanned in 2θ range from 30° to 120° with angle step 0.02° and exposition time 3 s. The Mössbauer spectra were recorded using a conventional POLON spectrometer with constant acceleration and the ^{57}Co source in a rhodium matrix. The spectrometer was calibrated using Fe foil. The diffraction pattern and Mössbauer spectra were obtained for samples in the form of thin ribbons using a fully automatic setup. Hyperfine parameters were derived using the NORMOS fitting program. Both, the Mössbauer spectra and X-ray patterns were recorded at room temperature.

The magnetic measurements at room temperature were performed by a LakeShore vibrating sample magnetometer with a maximum applied magnetic field of 2 T. Sample used for magnetic measurements had a ribbon shape of known dimensions. The demagnetization field resulting from its shape was taken into account and evaluated by the method described in [9].

Results and discussion

The analysis X-ray diffraction patterns of $Nd_{8.5}Tb_{1.5}Fe_{83}Zr_1B_6$ alloy in the as-cast state, revealed, that all obtained patterns were composed of halo and sharp peaks (Fig. 1a–c). The presence of such a halo is typically met in amorphous materials and the area below it, indirectly indicates a volume content of the amorphous phase in the alloy. The analysis of the positions and intensities of the sharp peaks at diffraction patterns were made using the EVA software by comparison with a PDF 2 database. Basing on these results it was found, that all peaks present on the XRD pattern can be assigned to the $(Nd,Tb)_2Fe_{14}B$ phase. The accuracy of the method and a large number of peaks originating from the $Nd_2Fe_{14}B$ phase of nanometric grain size, additionally broadened by the presence of Tb, does not allowed to reveal the presence of α-Fe phase, despite the excess amounts of Fe in the alloy composition.

Basing on qualitative X-ray studies, the presence of $Nd_2Fe_{14}B$ superstructure was revealed. Additionally, due to overstechiometric Fe content in alloy composition, the potential presence of α-Fe phase was also examined by the use of Mössbauer spectroscopy.

The Mössbauer spectra of partially crystallized alloys were treated as a superposition of spectra emanating from amorphous matrix and of situated therein crystalline phases.

For ordered, constituent phases, were assumed ratios of the intensities of particular components, corresponding to the ratio of crystallographically non-equivalent iron sites in the superstructure. In $Nd_2Fe_{14}B$, iron atoms occupy six non-equivalent positions, of the assignment ratio equal to 1:1:2:2:4:4. Therefore, parts of Mössbauer spectra resulting from presence of $Nd_2Fe_{14}B$ superstructure were described as a sum of six elementary Zeeman sextets of intensities, same as the assignment ratio of iron atoms in described elementary cell.

α-Fe superstructure was described by one elementary Zeeman sextet.

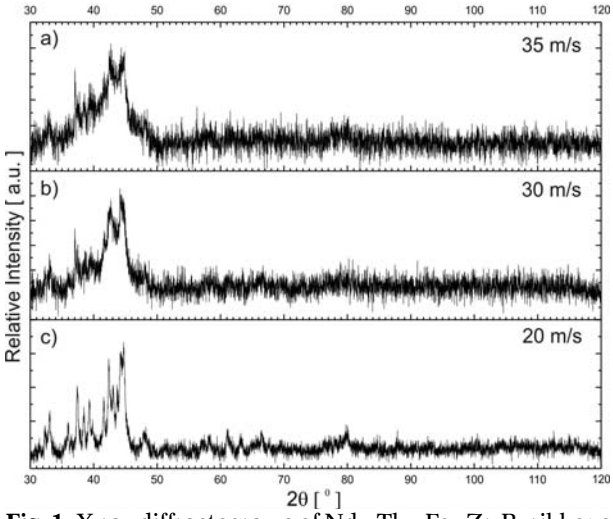

Fig. 1. X-ray diffractograms of $Nd_{8.5}Tb_{1.5}Fe_{83}Zr_1B_6$ ribbons in the as-cast state for samples produced at three different linear velocities (a) 35, (b) 30, and (c) 20 m/s.

For amorphous matrix, the finding probability of ^{57}Fe atoms in vicinity, characterized by B_m value of hyperfine field induction, was estimated by the method described in [10]. The applied method relied on approximation to continuous spectrum, of the amorphous matrix, a set of dozens Zeeman sextets with hyperfine fields B_i and isomeric shifts IS_i:

$$B_i = B_0 + i\Delta B, \quad IS_i = IS_0 + aB_i \tag{1}$$

where ΔB is the sharing step of variation area of hyperfine field induction (1 T), and a is the proportionality factor chosen in the approximation process.

The relative share of approximation sextets represents searched probability of finding iron surroundings of given Mössbauer parameters B_m, IS_m.

Moreover, it was assumed that the line intensity ratios in all Zeeman sextets were equal to $3:A_{2-5}:1:1:A_{2-5}:3$. The value of line intensity A_{2-5} was estimated in matching procedure and difference from value 2, was resulting from magnetic anisotropy. Samples used for measurements had ribbon shape and were obtained in rapid solidification process which can result in formation of mentioned anisotropies.

Figure 2 presents Mössbauer spectra of $Nd_{8.5}Tb_{1.5}Fe_{83}Zr_1B_8$ solidified at various speeds.

Basing on results obtained from the analysis of Mössbauer spectra it was found that all measured samples had multiphase structure composed from two superstructures: $Nd_2Fe_{14}B$ and α-Fe dispersed in amorphous matrix. The α-Fe phase content was so small, that its presence was not detected by X-ray studies. The relative content of the superstructures V_n of ordinal number n was estimated from the formula:

$$V_n = \frac{R_n \cdot c_{\mathrm{Fe}}}{R \cdot c_{\mathrm{Fe},n}} \tag{2}$$

where R_n meant surface part of the spectrum attributed to the superstructure, R was the total area of the spectrum, c_{Fe} was the concentration of iron atoms in the sample, $c_{Fe,n}$ was the concentration of iron atoms in superstructure.

The relative content of the amorphous matrix V_{am} was estimated by the formula:

$$V_n = 1 - \left(V_{\mathrm{Fe}} + V_{\mathrm{Re_2\,Fe_{14}B}}\right) \tag{3}$$

and the concentration of iron atoms in it by the formula:

$$_{\mathrm{Fe},am} \quad \frac{R_{am} \cdot c_{\mathrm{Fe}}}{R \cdot V_{am}} \tag{4}$$

Selected results obtained from the matching of Mössbauer spectra, and determined using Eqs. (2)–(4) are summarized in Table 1.

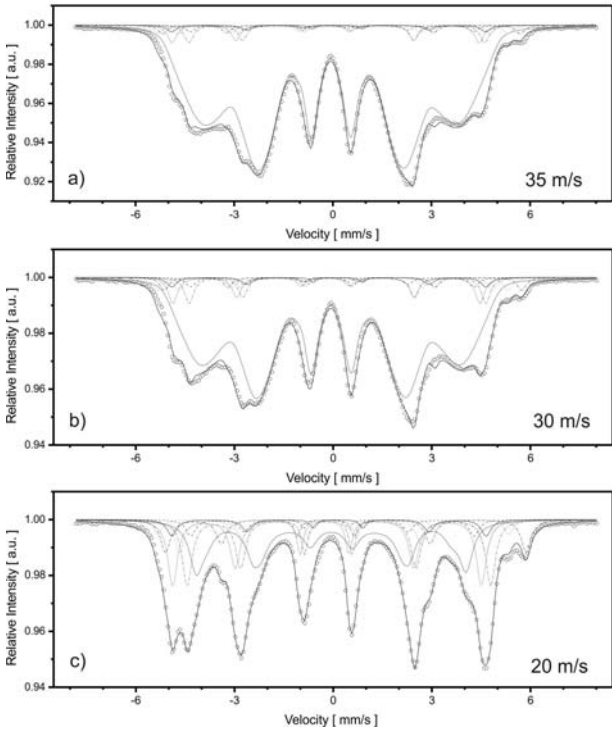

Fig. 2. Mössbauer spectra of $Nd_{8.5}Tb_{1.5}Fe_{83}Zr_1B_8$ ribbons in the as-cast state for samples produced at three different linear velocities (a) 35, (b) 30, and (c) 20 m/s.

As can be seen from data collected in Table 1, the slower the linear speed of copper wheel, the slower is the crystallization process and the higher is the content of the crystalline phases. This in turn results in a reduction of the B and Re content in a volume of the amorphous matrix, which is confirmed by the higher value of $B_{\mathrm{eff,Am}}$ and an increase in Fe content in amorphous matrix.

In Fig. 3 are presented the initial magnetization curves and major hysteresis loops measured for all investigated samples.

The sample solidified with the lowest cooling rate was characterized by a smooth single-course hysteresis loop. This behavior, together with the multi-phase structure of the sample (two phases with different magnetic hardness), demonstrates a strong coupling of the magnetic moments of both phases by short-range exchange interactions [11–13]. Samples solidified with higher cooling rates, have magnetic properties typical for the half-hard magnetic materials and the shape of the wasp-waist hysteresis loop. Such a type of hysteresis loop was attributed by [14] to materials with grains of crystalline phase fine dispersed in amorphous matrix.

Table 1. The set of parameters determined from the matching of Mössbauer spectra for all studied samples

Linear velocity of copper wheel [m/s]	A_{2-5} line intensity [a.u.]	Phase content			$B_{\mathrm{eff,\,Am}}$ [T]	Fe content in amorphous matrix
		$Re_2Fe_{14}B$ [%]	α-Fe [%]	amorphous [%]		
20	2.67(3)	66	3	31	22.66	83.2
30	2.38(2)	21	2.5	66.5	22.45	82.6
35	2.48(1)	13	1.5	85.5	22.15	80

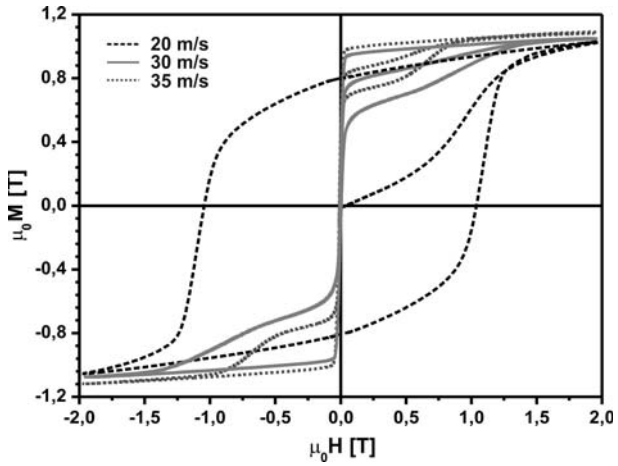

Fig. 3. Major hysteresis loops and virgin magnetization curves of $Nd_{8.5}Tb_{1.5}Fe_{83}Zr_1B_8$ ribbons in the as-cast state for samples produced at three different linear velocities 35, 30, and 20 m/s.

Conclusion

The analysis X-ray diffraction patterns of $Nd_{8.5}Tb_{1.5}Fe_{83}Zr_1B_6$ alloy in the as-cast state, revealed that studied material was composed of the $(Nd,Tb)_2Fe_{14}B$ phase dispersed in amorphous matrix. The accuracy of the method and a large number of peaks originating from the $Nd_2Fe_{14}B$ phase of nanometric grain size, additionally broadened by the presence of Tb, do not allow to reveal the presence of α-Fe phase, despite the presence of excess amounts of Fe in the alloy composition.

The analysis of Mössbauer spectra, revealed that all measured samples had multiphase structures composed from two superstructures: $Nd_2Fe_{14}B$ and α-Fe dispersed in amorphous matrix. The α-Fe phase content was so small, that its presence was not detected by X-ray studies. Additionally, it was shown that the slower the linear speed of copper wheel, the slower is the crystallization process and the higher is the content of the crystalline phase. This in turn results in a reduction of the B and Re content in a volume of the amorphous matrix, which was confirmed by the higher value of $B_{\mathrm{eff,Am}}$ and an increase in Fe content in amorphous matrix.

The 66% content of Re-Fe-B phase resulted in strong exchange coupling between amorphous matrix and $Re_2Fe_{14}B$ grins, what in turn resulted in good hard magnetic properties. Materials produced at higher linear speeds of copper drum were composed of too small amounts of the magnetically hard phase, to form a strong coupling between the amorphous matrix and $Re_2Fe_{14}B$ grains. Observed hysteresis loops had wasp–waist shape, and samples had half-hard magnetic properties.

References

1. Kronmuller, H., Fischer, R., Bachmann, M., & Leineweber, T. (1999). Magnetization processes in small particles and nanocrystalline materials. *J. Magn. Magn. Mater., 203*, 12–17. DOI:10.1016/S0304-8853(99)00184-5.
2. Hono, K., & Sepehri-Amin, H. (2012). Strategy for high-coercivity Nd-Fe-B magnets. *Scr. Mater.*, *67*, 530–535. DOI:10.1016/j.scriptamat.2012.06.038.
3. Dospial, M., Plusa, D., & Slusarek, B. (2012). Study of the magnetic interaction in nanocrystalline Pr-Fe--Co-Nb-B permanent magnets. *J. Magn. Magn. Mater.*, *324*, 843–848. DOI:10.1016/j.jmmm.2011.09.029.
4. Kronmuller, H., & Bachmann, M. (2001). Magnetization processes in nanocrystalline assemblies of particles. *Physica B*, *306*, 96–101. DOI:10.1016/S0921-4526(01)00985-1.
5. Liu, J., Sepehri-Amina, H., Ohkuboa, T., Hioki, K., Hattori, A., Schrefl, T., & Hono, K. (2013). Effect of Nd content on the microstructure and coercivity of hot-deformed Nd-Fe-B permanent magnets. *Acta Mater.*, *61*, 5387–5399. DOI:10.1016/j.actamat.2013.05.027.
6. Ceglarek, A., Płusa, D., Dośpiał, M., Nabiałek, M., & Wieczorek, P. (2013). Magnetic properties and surface domain structure of $(Nd_{0.85}Dy_{0.15})_{10}Fe_{83}Zr_1B_6$ thin ribbons. *Opt. Appl., 43*, 117–122. DOI: 10.5277/oa130115.
7. Hu, Z. H., Lian, F. Z., Zhu, M. G., & Li, W. (2008). Effect of Tb on the intrinsic coercivity and impact toughness of sintered Nd-Dy-Fe-B magnets. *J. Magn. Magn. Mater.*, *320*, 1735–1738. DOI:10.1016/j.jmmm.2008.01.027.
8. Pinkerton, F. E. (1986). High coercivity in melt-spun Dy-Fe-B and Tb-Fe-B alloys. *J. Magn. Magn. Mater.*, *54/57*, 579–582. DOI:10.1016/0304-8853(86)90716-X.
9. Panda, A. K., Basu, S., & Mitra, A. (2003). Demagnetisation effect and its correction on the measurement of magnetic hysteresis loop of melt-spun ribbons. *J. Magn. Magn. Mater.*, *261*, 190–195. DOI:10.1016/S0304-8853(02)01472-5.
10. Ciurzynska, W. H., Varga, L. K., Olszewski, J., Zbroszczyk, J., & Hasiak, M. (2000). Mössbauer studies and some magnetic properties of amorphous and nanocrystalline $Fe_{87-x}Zr_7B_6Cu_x$ alloys. *J. Magn. Magn. Mater., 208*, 61–68. DOI:10.1016/S0304-8853(99)00569-7.
11. Dospial, M., & Plusa, D. (2013). Magnetization reversal processes in bonded magnets made from a mixture of Nd-(Fe,Co)-B and strontium ferrite powders. *J. Magn. Magn. Mater.*, *330*, 152–158. DOI:10.1016/j.jmmm.2012.10.022.
12. Plusa, D., Slusarek, B., Dospial, M., Kotlarczyk, U., & Mydlarz, T. (2006). Magnetic properties of anisotropic Nd-Fe-B resin bonded magnets. *J. Alloy. Compd.*, *423*, 81–83. DOI:10.1016/j.jallcom.2005.12.051.
13. Plusa, D., Dospial, M., Slusarek, B., & Kotlarczyk, U. (2006). Magnetization reversal mechanisms in hybrid resin-bonded Nd-Fe-B. *J. Magn. Magn. Mater.*, *306*, 302–308. DOI:10.1016/j.jmmm.2006.03.032.
14. Martínez-García, J. C., García, J. A., & Rivas, M. (2008). Asymmetric magnetization reversal of partially devitrified $Co_{66}Si_{15}B_{14}Fe_4Ni_1$. *J. Non-Cryst. Solids*, *354*, 5123–5125. DOI:10.1016/j.jnoncrysol.2008.05.059.